The Effect of Human Tissue on Field Strength Measurements In Vivo Using a Resonant UHF Cavity-Backed Slot Antenna

Noor M. Albadri[1], **Julie A. Hides**[2], **Hugo G. Espinosa**[1]* and **David V. Thiel**[1]

[1]*School of Engineering and Built Environment, Griffith University, Nathan Campus, Brisbane, Queensland, Australia*
[2]*School of Allied Health Sciences, Griffith University, Nathan Campus, Brisbane, Queensland, Australia*

An inward-looking wearable antenna can be used for radio communications with internal transceivers in vivo. The radio transmissions are recorded using an array of electric field sensors on the skin. This paper reports the effect of living tissue on a small cavity-backed slot antenna pressed onto soft tissue of the human torso at 2.09 GHz. In-vivo measurements were made on the skin surface at 13 torso locations using eight participants (age range, 22–68 years old), with body mass index ranging between 20.3 and 31.6 kg/m^2. Ultrasound imaging was used to determine the skin and fat thickness at every measurement location. The variation in the antenna input impedance measurements demonstrated that the human tissues (fat and muscle) affect the antenna impedance but the mismatch creates field strength measurement errors of less than 2 dB. Fat thickness in the range of 3–30 mm can slightly degrade the performance of these wearable antennas. These effects can be partly mitigated by selective location and antenna retuning to improve transceiver communications. Bioelectromagnetics. 2021. © 2021 Bioelectromagnetics Society

Keywords: **wearable antennas; slot antennas; human tissue; ultrasound; field strength**

INTRODUCTION

Over the past decade, wearable antennas have attracted significant attention due to the wide range of potential applications in several fields (e.g., medical, sports, and military). In these applications, the antenna operates in close proximity or directly attached to the human body, which introduces a specific requirement for a compact wearable antenna design [Arif et al., 2019; Tajin et al, 2019]. This requirement includes small, lightweight, robust, easy to manufacture, and ideally conformal to the body surface, yet they must maintain high performance in terms of reliability and efficiency [Agneessens et al., 2015].

This paper shows that the body-worn antenna characteristics are affected by the electromagnetic and anatomical parameters of the individual wearing the antenna. These parameters vary at different locations on the same person and from one person to another [Agarwal et al., 2016]. The antenna performance is significantly modified by the human body proximity [Ashyap et al., 2017; Sabban, 2019]. The placement of these antennas on the body depends on the application. There are three common uses for wearable antennas on the human body: off-body communications, on-body communications, and in-body communications.

Off-Body Antennas

These are used to communicate with other devices such as base stations far away from the body [Zhu et al., 2016]. The antennas are located on the human body and designed to communicate externally to their surrounding environment [Ruiz et al., 2019]. An example of this is a wearable ultra-high frequency (UHF) slot antenna developed for sports applications [Fernández et al., 2018a]. In this study, in-vivo measurements were performed,

Conflicts of interest: None.

*Correspondence to: Hugo G. Espinosa, School of Engineering and Built Environment, Griffith University, Nathan Campus, 170 Kessels Rd, Nathan, Brisbane, QLD 4111, Australia.
E-mail: h.espinosa@griffith.edu.au

Received for review 4 June 2020; Accepted 23 February 2021

DOI:10.1002/bem.22331
Published online 00 Month 2021 in Wiley Online Library (wileyonlinelibrary.com).

together with numerical simulations on a voxel body model in different body locations.

On-Body Antennas

These are directly attached to the human body and operate in close proximity with other body-worn or implanted antennas [Miah et al., 2019; Paracha et al., 2019]. The near-surface properties of the skin can affect the radio field propagation and the antenna performance [Kissi et al., 2019].

Mapping the layers immediately beneath the antenna can be accurately undertaken using ultrasound imaging. This technique has been demonstrated to be a highly accurate method (<1 mm) of determining the dimensions (thickness and extent) of soft tissue by comparison with magnetic resonance images [Hides et al., 1995]. Another example of this type of antenna includes an inward-facing slot antenna [Fernández et al., 2018b], manufactured using three-dimensional (3D) printing and selectively coated with conducting ink silver paste. The slot was fed using a capacitively coupled feed probe inside the box and connected via coaxial cable. The antenna was tuned to 2.45 GHz when placed on the skin of a human torso, and it was developed for gastrointestinal radio pill tracking at 2.45 GHz [Fernández et al., 2018b]. In addition, computation of radiofrequency (RF) energy absorption in human bodies at 2.4 GHz using two on-body antennas for off-body and in-body radiation was presented in Fernández et al. [2020].

In Albadri et al. [2020], the authors examined the effect of coupling between two identical human torso body-worn antennas and the effect of an external radio source at 2.1 GHz. The results showed a reduced signal-to-noise ratio of 75 dB at 2.1 GHz.

In-Body Antennas

These are embedded or located inside the body and communicate to on-body antennas [Kiourti and Nikita, 2017]. One application includes radio endoscopy, where a radio pill is used to investigate the gastrointestinal tract (GI) [Caffrey et al., 2008; Arefin et al., 2018]. In this scenario, the surface antenna is inwardly directed, and so is far more susceptible to variations in the electromagnetic properties of the intervening tissues. Deneris et al. [2019] reported impedance measurements and frequency shifts for a strip dipole antenna at 433 MHz on a layered pork sample in-vitro.

RESEARCH OUTLINE

In this study, a slot antenna matched to human soft tissue on the torso (minimum S_{11}) to a 50 Ω transmission line was used as a wearable sensor for field strength measurements from an ingested radio transmitter. When the match is not perfect, the received signal strength decreases. The reflection coefficient S_{11} allows calculation of the transmissivity S_{21} (Fig. 1). Of importance in field strength measurements is the fact that for $S_{11} < -4$ dB, the field strength measurement will be reduced by 2 dB. This lies within the variations of most in-vivo measurements as outlined in this paper. Here, we report these

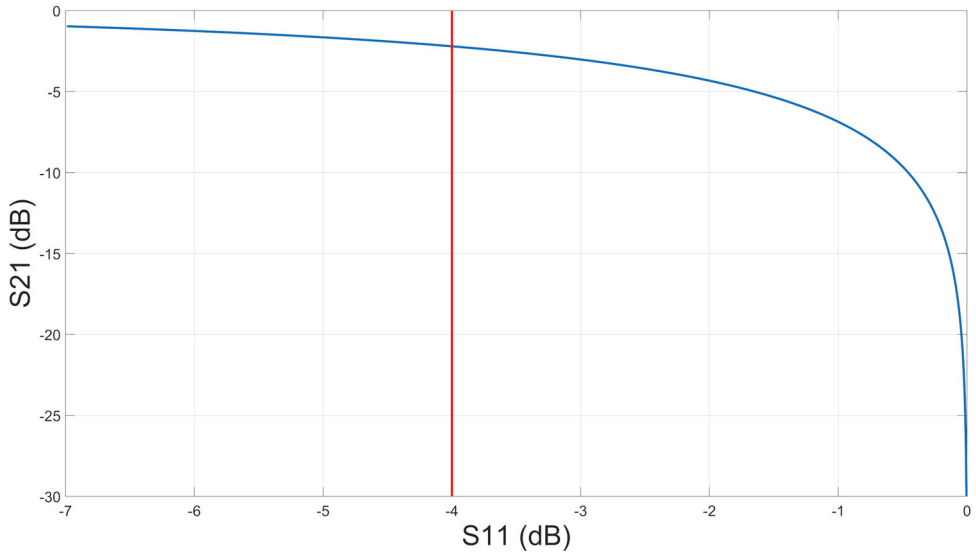

Fig. 1. True field and received field (transmission loss S_{21}) as a function of the antenna mismatch (S_{11}) to a 50 Ω cable. Note that for $S_{11} < -4$ dB (red vertical line), the received field is reduced by 2.2 dB.

TABLE 1. The Electromagnetic Properties of the Different Tissue Layers at 2.45 GHz [Gabriel, 1996] Used in Finite-Difference Time-Domain Modeling

Frequency (GHz)	Tissue name	Conductivity, σ (S/m)	Relative permittivity, ε_r	Loss tangent, tanδ
2.45	Skin dry	1.464	38.007	0.283
	Fat	0.104	5.280	0.145
	Muscle	1.739	52.729	0.242

variations measured and modeled on 13 body locations and on 8 participants with different body mass index (BMI), using both numerical modeling and in-vivo human measurements. This type of measurement and analysis has not previously been reported.

METHODOLOGY

This study focused on measuring and modeling the antenna impedance at different torso locations and with a number of human subjects.

Three complementary approaches were used: (i) the effect of muscle/fat/skin variations on the antenna impedance of an inward-facing slot antenna on the skin surface was explored using numerical modeling; (ii) the input impedance of the slot antenna was measured on human torsos for eight subjects with different body types; (iii) for comparison, the ultrasound thickness (skin, fat, and soft tissue of the torso) measurements of the eight participants were used to model the antenna impedance on multi-layered skin.

The finite-difference time-domain (FDTD) using a commercially available software suite (CST Studio Suite, www.3ds.com/products/simulia)) was used for all numerical computations. The material library available with this software includes the electromagnetic properties of many different tissue types. The physiological properties of the human tissue can be represented by the intensity of the electric and magnetic fields, and their directional characteristics [Salgado et al., 2004]. Any variations in the normal tissue structures (caused by biological variations) result in different electromagnetic field parameters, which are frequency-dependent. A multilayer human skin model represented by three main layers (skin, fat, and muscle) was designed to imitate the characteristics of living human skin at 2.45 GHz.

The effective dielectric properties (conductivity and relative permittivity) of the skin layers were calculated using the electromagnetic properties given in Table 1. These properties were measured and reported from RF to Terahertz frequencies by several research groups [Gabriel, 1996; Salgado et al., 2004; Miklavcic et al., 2006; Agarwal et al., 2016; Baghaee and Mohassel, 2016; Hassan, 2018].

Cavity-Backed Slot Antenna

The antenna was matched to the 50 Ω feed cable at 2.45 GHz for maximum accuracy of the field strength measurements. Simulations were performed to improve the antenna performance on human tissue assuming a planar multilayer tissue structure using a cavity-backed slot antenna [Fernández et al., 2018a]. The radiation as a function of distance for a cavity slot antenna was reported by Lin [1974] for biological applications. Although the antenna was modified to operate at a resonant frequency f_0 of 2.45 GHz with a reflection coefficient <-20 dB when placed on the skin, in experimental measurements this antenna had a resonant frequency of approximately 2.09 GHz. In air, there was a slight shift difference in the resonant frequency between the experimental measurement and CST simulation results. The measured resonant frequency was 6.92 GHz with a reflection coefficient $S_{11} < -10$ dB (see Fig. 2).

The antenna consists of an aluminum box with a resonant slot internally coupled with a monopole probe and coaxial cable. The slot antenna is linearly polarized with the E-field parallel to the long axis of the box (perpendicular to the slot). The box and lid were machined from an aluminum block (see Fig. 3).

The box's outer dimensions were $33 \times 33 \times 11\ mm^3$ and the wall thickness was 1.5 mm as shown in Figure 3a. The antenna slot dimensions were $21 \times 9 \times 1.5\ mm^3$, and the distance from the slot to the feeding probe was 6 mm (see Fig. 3b). The rectangular probe was made from a brass sheet (conductivity 1.59×10^7 S/m). The brass probe (dimensions $21.50 \times 5 \times 0.1\ mm^3$) was soldered to the 50 Ω SubMiniature version A (SMA 8500-0000; RF Shop, Lonsdale, Australia) connector (see Fig. 3c and d).

The antenna impedance at resonance was determined using numerical modeling from the minimum S_{11} value with the antenna resting on a three-layer model (skin, fat, and muscle) (Fig. 4). The electromagnetic properties of these tissue layers are given in Table 1. The fat layer thickness

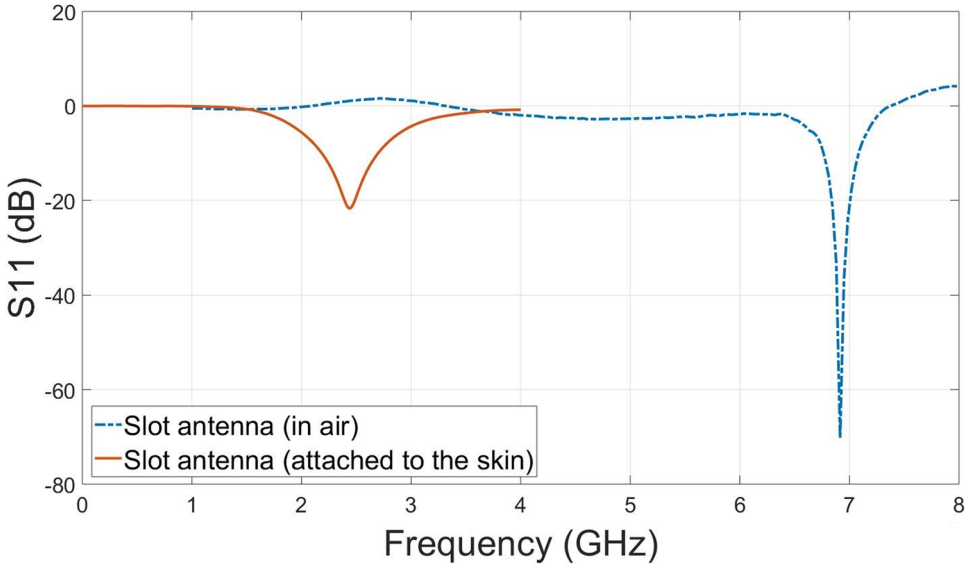

Fig. 2. Antenna reflection coefficient S_{11} for free space 6.92 GHz (dashed blue line) and 2.45 GHz against the skin (solid red line).

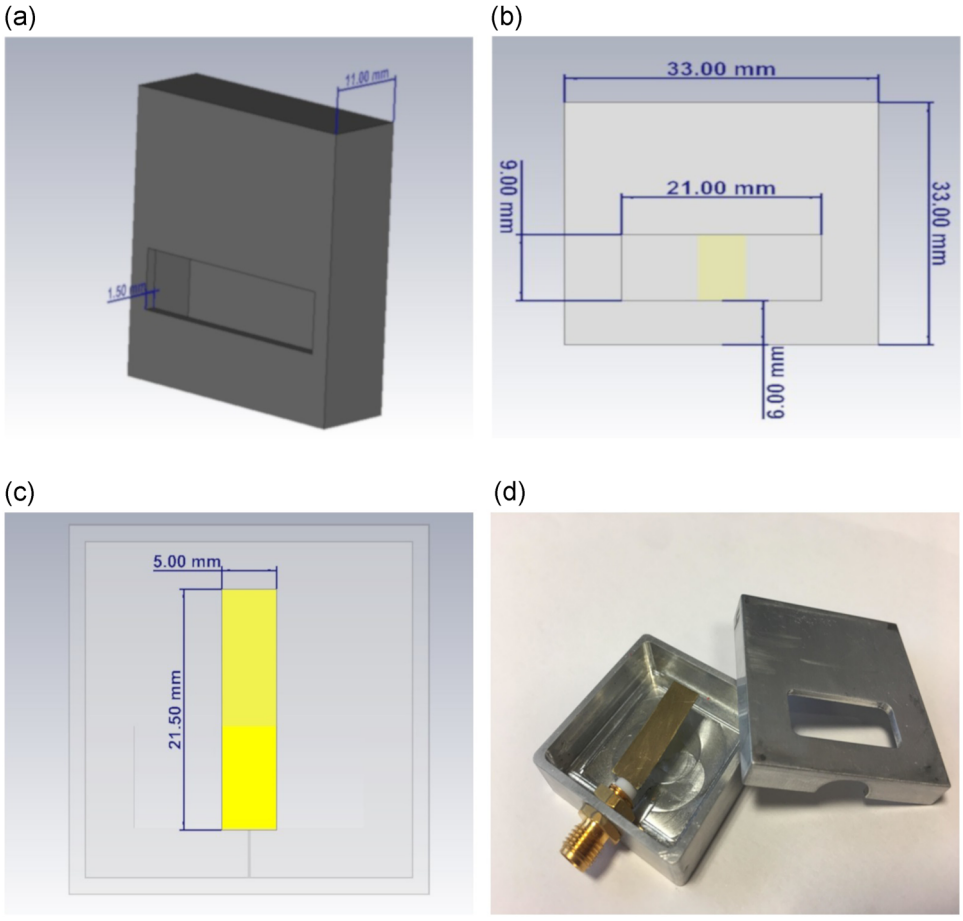

Fig. 3. Monopole slot antenna. (**a**) Model antenna design. (**b**) Box and slot dimensions. (**c**) Monopole antenna dimensions. (**d**) Antenna prototype with a 50 Ω SMA connector.

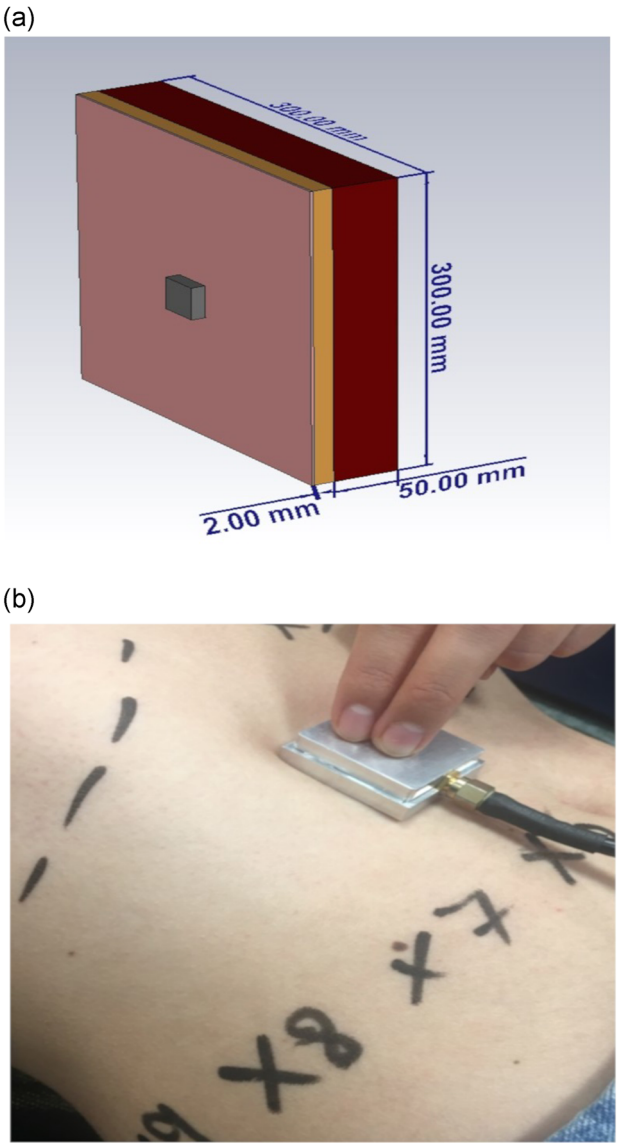

Fig. 4. (**a**) Slot antenna in direct contact with the three-layer human tissue model (pink layer: skin, orange layer: fat, and red layer: muscle). (**b**) Participant with the inward antenna at different body locations.

was varied between 0 and 70 mm, with a constant skin thickness of 2 mm and a lower layer of muscle of 50 mm.

In all simulations and measurements, the slot antenna was in direct contact with the human tissue (see Fig. 4). Although significant change is evident in the resonant frequency as the fat layer thickness is increased (Fig. 5a), when the fat thickness is greater than 40 mm there is little change.

The area of the skin model used in the numerical calculations was $300 \times 300\,\text{mm}^2$. This area and the muscle thickness are large enough to appear infinite for the S_{11} modeling. The operator's hand holding the antenna in the position of a participant was found not to influence the S_{11} measurements. The finger pressure was low enough to maintain full antenna contact with the skin without participant discomfort.

When the fat thickness was small (<5 mm), the antenna match was poor and $S_{11} > -5$ dB (Fig. 5b). A poor match results in a decrease in the received signal (Fig. 1). It was also observed that the average resonant frequency was slightly below the desired Industrial, Scientific, and Medical frequency band (ISM) of 2.45 GHz (2.088 GHz).

In-Vivo Experimental Measurements

Experimental measurements were made on eight participants of different ages, gender, and BMI as listed in Table 2. All volunteers were subjected to S_{11} measurements using both a vector network analyzer (VNA) and ultrasound imaging at 13 different locations on the torso. These locations were selected to avoid nearby bone. The trials were conducted in accordance with Griffith University's ethics research committee (Ethics approval number GU ref no: 2018/601).

Ultrasound imaging. The soft tissue thickness values of skin and fat of the trunk for the 13 trunk locations (see Fig. 6) were determined directly from the ultrasound images. Ultrasound imaging provided precise morphological information on anatomical structures [Hassan, 2018]. For the trunk region, the validity of the imaging protocol used was previously established by comparison with Magnetic Resonance Imaging, which is known as the "gold standard" of musculoskeletal imaging due to its excellent soft-tissue contrast [Hides et al., 1995].

The ultrasound imaging apparatus (GE LOGIQ e ultrasound unit—General Electric Healthcare, Waukesha, WI) was equipped with a 5 MHz convex array transducer. Participants were initially positioned in supine lying with their knees flexed (for imaging of the anterior locations) and then positioned in prone lying (for imaging of posterior trunk locations).

The 13 locations listed in Table 3 were marked on the skin with a marker. For the anterior sites, the inferior margins of the rib cage and superior margins of the iliac crest were first palpated and used as landmarks (see Fig. 6a). Posteriorly, the spinous processes of the L3, L4, and L5 were used as landmarks (see Fig. 6c), to avoid imaging over bony structures (iliac crest), and to avoid interference from bone, as the bone has a significantly different electromagnetic conductivity. Participants were instructed to relax the abdominal and paraspinal

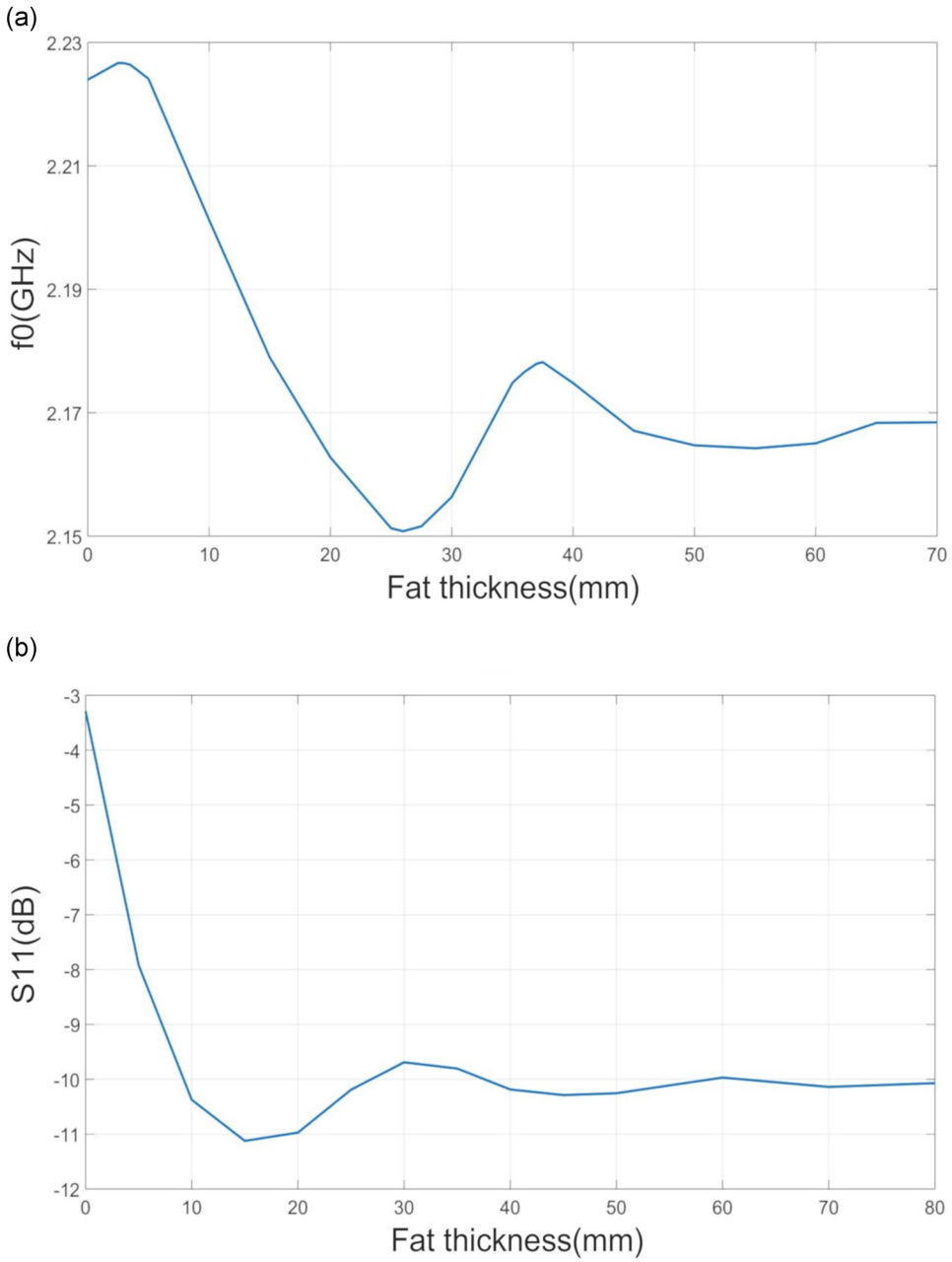

Fig. 5. (**a**) Resonant frequency f_0 (GHz) versus fat thickness (mm). (**b**) Reflection coefficient S_{11} (dB) versus fat thickness (mm).

muscles, the gel was applied, and the transducer was positioned over the marked locations to obtain images of the soft tissue. Ultrasound images were stored offline and OsiriX medical imaging software (Geneva, Switzerland) was used for image visualization and measurement. Measurements were made in the midline of the image, perpendicular to the layers of soft tissue.

Figure 7 shows an example of the ultrasound image at location number 5 on participant number 5. The distances between the skin surface and boundaries of the layers of soft tissue can be accurately determined to within 0.1 mm.

VNA measurements. The slot antenna measurements (f_0, S_{11}) were recorded using a 50 Ω VNA. To assess the reproducibility of the S_{11} measurements, the antenna was repeatedly placed 20 times at the same position on the abdominal area (location 4) of one

TABLE 2. Characteristics of the Participants Used in This Study

Participant	Gender	Age	Mass (kg)	BMI	Height (cm)	Waist circumference (cm)	Last major meal (h)
1	Male	68	93	29.02	179	97	2
2	Female	26	52.6	20.29	161	71	4
3	Male	33	89.2	31.6	168.8	110	3
4	Male	22	76.5	22.94	182.7	92	2
5	Male	61	85.6	26.71	179.5	96 spleen removed	4
6	Male	42	83.9	25.05	183.2	97	14
7	Male	22	85.8	28.66	173	89	16
8	Male	22	91.3	25.29	190	91	3

BMI = body mass index.

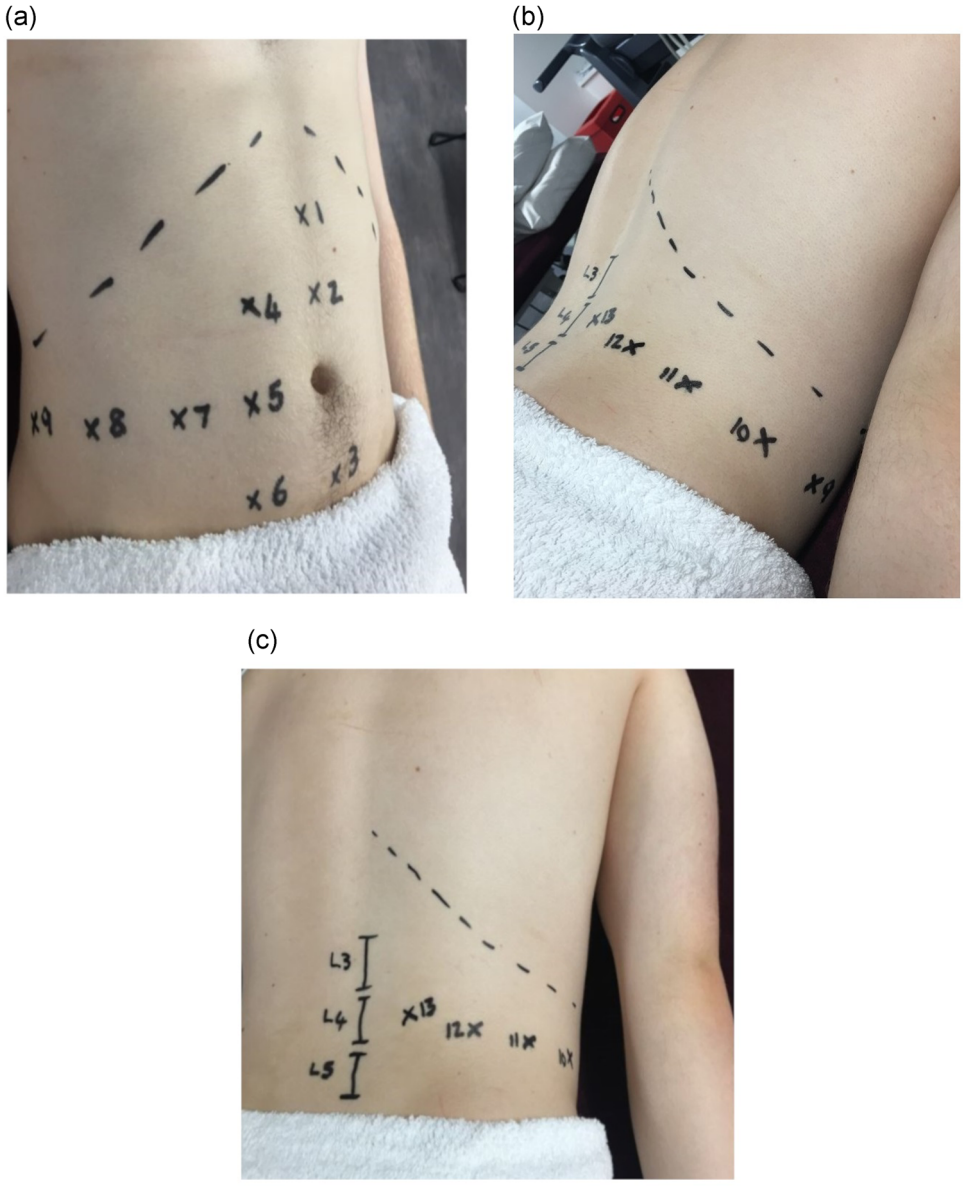

Fig. 6. Human torso figure used to indicate the locations of the measurement points. (**a**) Anterior view. Dotted lines indicate inferior margins of the rib cage. (**b**) Lateral view. (**c**) Posterior view, with L3, L4, and L5 spinous processes marked as landmarks.

TABLE 3. Locations and Description of the Measurement Sites (Fig. 6)

Location	Description
(1–3)	Marked along the midline of the abdominal wall, in a superior/inferior orientation in line with the umbilicus
(4–6)	Marked along a line parallel and lateral to the midline
(7–8)	Horizontally aligned with location 5 and the umbilicus
(9–13)	Horizontally aligned with location 8, ensuring that the posterior locations were superior to the iliac crest (L4-5 interspace)

participant. The results showed a root mean standard deviation of 0.0141 GHz in the resonant frequency, which is small compared with the bandwidth error bars of −3 dB.

Figure 8 compares the simulated and measured S_{11} values for one of the participants in one location (location 5). The differences between the simulation and experiment results are due to the complex human structure and the variations in the dielectric properties of the human tissue between the participants. The −10 dB bandwidth of the antenna was approximately 0.7 GHz (28%) but varied with anatomical location and was different for each participant.

To distinguish the error percentage of the simulations and VNA measurement results between each case, the 3 dB bandwidth error bar was used (see Fig. 9). A slight variance in the resonant frequency range 0.1-0.3 GHz was observed across all participants. In the simulations, the thickness of the layers of the skin, fat, and muscle captured in the ultrasound image was used. The differences between the FDTD modeling (CST) and the VNA measurements most likely relate to the more complex human structure (e.g., muscle orientation, fascial tissue, blood, nerves, fluids, etc.) as well as the planar structure of the model.

The S_{11} results from the simulations and VNA measurements for all thirteen locations are summarized in box and whisker plots in Figure 10a and b. The median value and the upper and lower

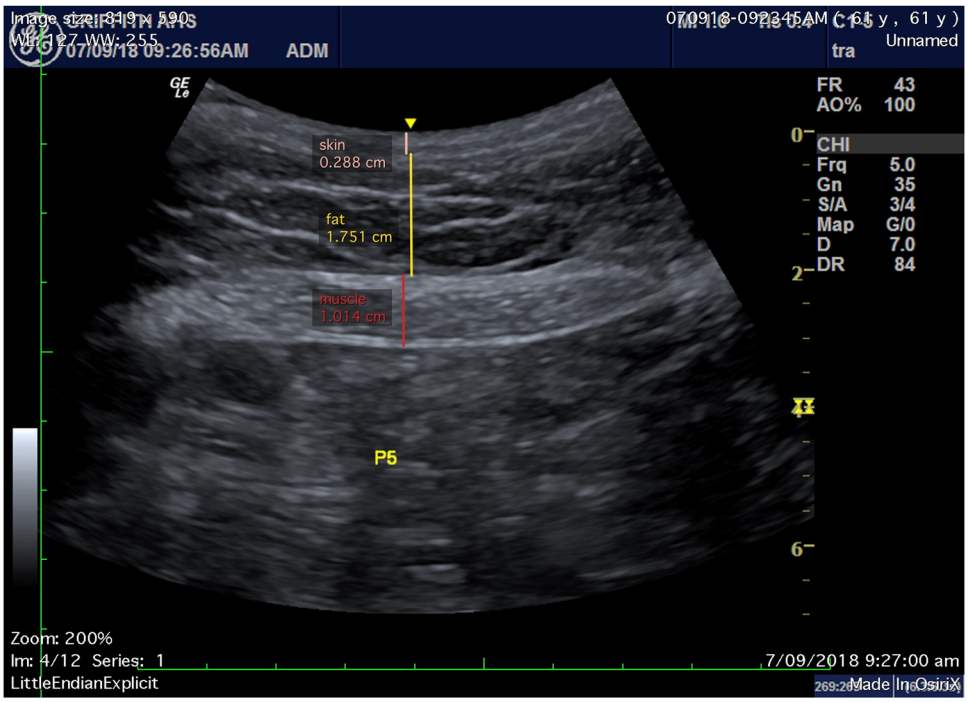

Fig. 7. Transverse ultrasound image (skin, fat, and muscle) in position 5 from participant number 5. The pink line shows the skin thickness (2.88 mm), the yellow line shows the fat thickness (17.51 mm), and the red line shows the muscle layer thickness of the rectus abdominis muscle (10.14 mm).

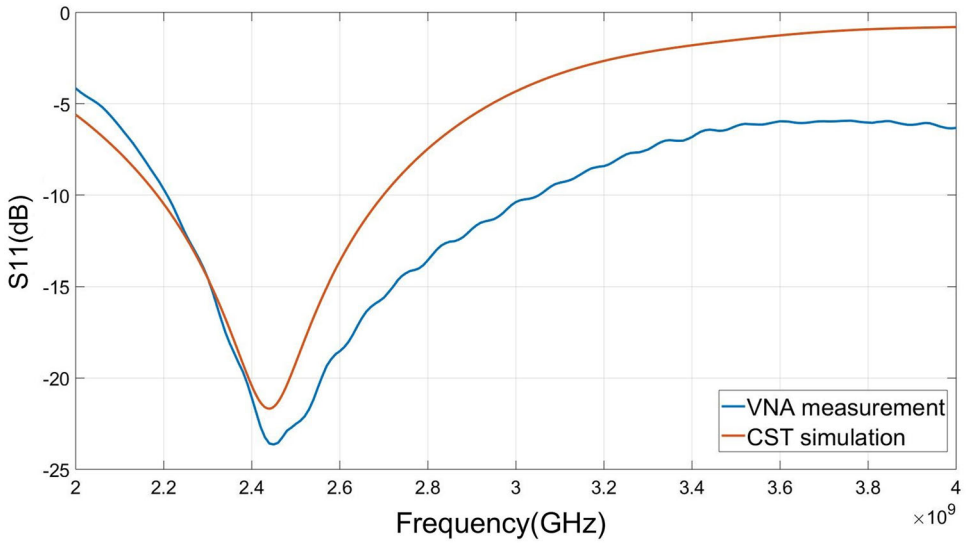

Fig. 8. Comparison between the finite-difference time-domain simulation and measurement of the slot antenna, using the layer thickness data determined from the thickness measurements of the ultrasound.

quartiles are marked in the plot. In the VNA measurements (Fig. 10a), it is evident that 97% of the points lie below the S_{11} value of −4 dB, which translates to the S_{21} accuracy of the transmissivity of better than −2 dB. The CST S_{11} values (Fig. 10b) are slightly smaller due to the complex structure of the human body, but the variations between individuals are not highly correlated. In addition, to mitigate the effect of the complex structure of the human abdomen torso on the input impedance of the cavity-backed slot antenna, S_{11} for the 8 participants at the 13 locations was investigated (Fig. 11). It can be seen that the antenna performance at locations 1, 4, 6, and 7 (lower S_{11} median values) was better than at the other locations, due to the structure of the multilayer tissue of the human body (skin, fat, and muscle), and to the thickness of the fat and muscle layers at these positions.

The relationship between the average resonant frequency for an individual and their average fat thickness is shown in Table 4. The Pearson correlation coefficient shows no significant relationship between the average resonant frequency and average fat thickness ($r^2 = 0.07$), age ($r^2 = 0.016$), and BMI ($r^2 = 0.11$) of the participants.

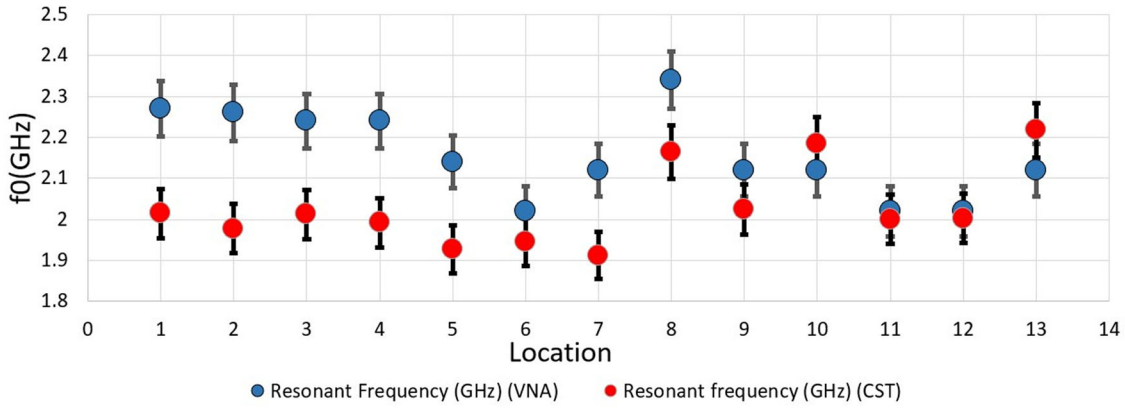

Fig. 9. 3 dB bandwidth error bar distinguishes the variation in the antenna resonant frequency f_0 at all locations for one participant.

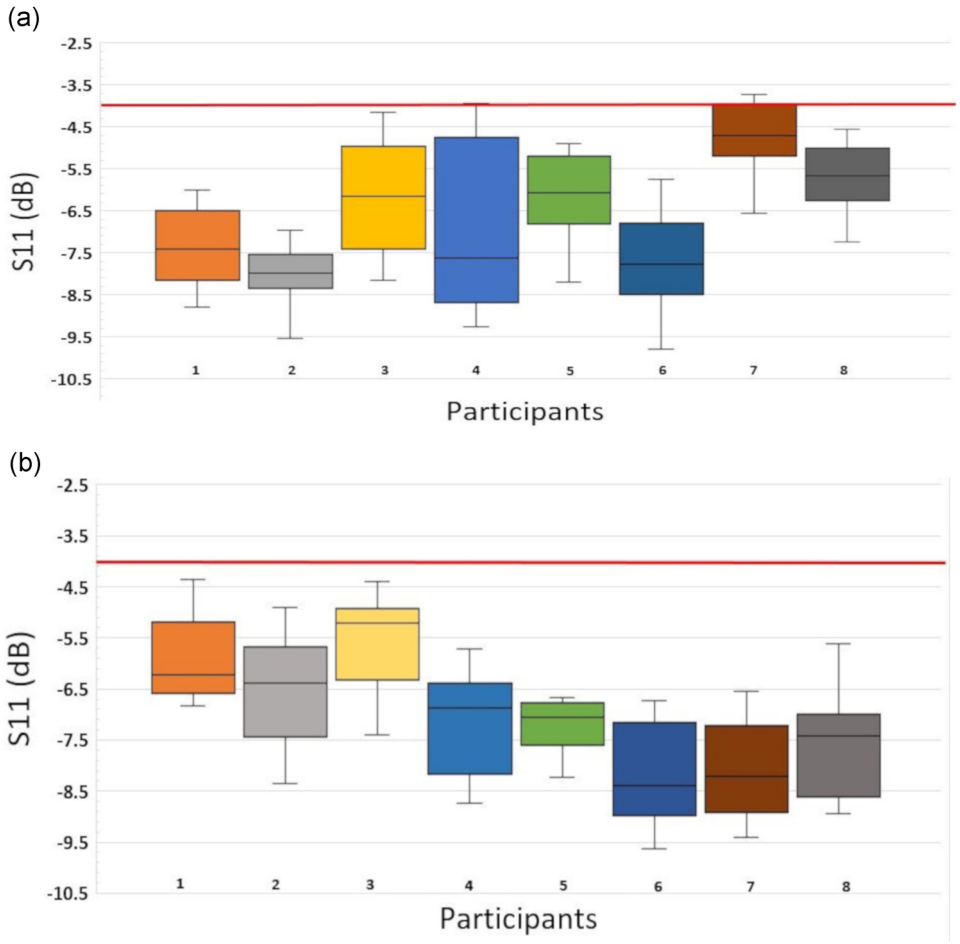

Fig. 10. (**a**) Mean S_{11} values and quartile ranges for the 8 participants at 2.088 GHz (vector network analyzer [VNA] measurements). Note that almost all (97%) S_{11} values are less than –4 dB as indicated by the red horizontal solid line. (**b**) Mean S_{11} values and quartile ranges for the 8 participants based on the ultrasound thickness measurements at 2.079 GHz (finite-difference time-domain model simulations). Note that all S_{11} values are less than –4 dB as indicated by the red horizontal line.

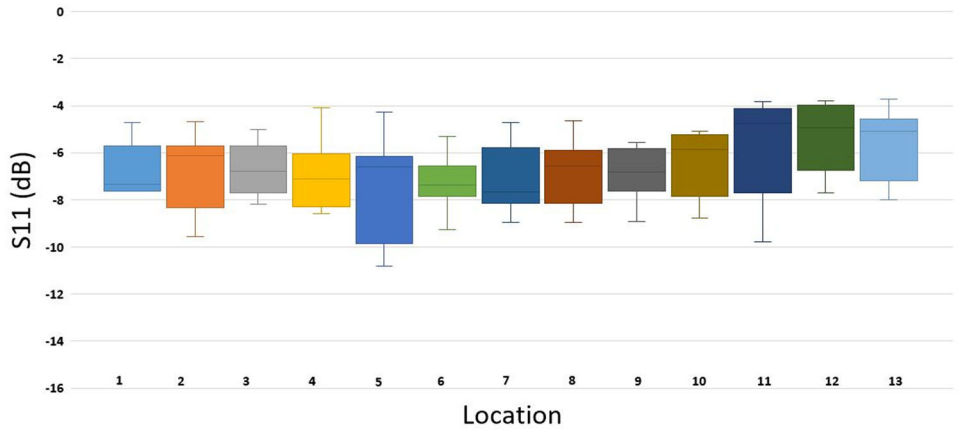

Fig. 11. S_{11} in dB for the 8 participants at the 13 locations.

TABLE 4. Mean and Standard Deviation Values of the Measured Resonant Frequency and the Fat Thickness for All Participants

Participant	Average, f_0 (GHz)	Average fat thickness (mm)
1	2.16 (0.11)	15.5 (6.87)
2	2.14 (0.09)	11.0 (3.13)
3	2.00 (0.09)	21.1 (7.75)
4	2.03 (0.13)	10.0 (3.23)
5	2.00 (0.10)	15.8 (4.85)
6	2.21 (0.13)	14.3 (4.02)
7	2.04 (0.14)	10.1 (4.10)
8	2.14 (0.14)	8.97 (4.41)

CONCLUSION

Antenna impedance measurements on 8 participants were compared with FDTD planar numerical models developed from thickness measurements obtained from ultrasound images of the torso. From these measurements, it was concluded that the antenna input impedance is consistent at a fixed location for an individual, but that the impedance varies significantly between torso locations and individuals. This variation is not predictable; however, the effect on the field strength measurements is relatively small. The antenna bandwidth is sufficient (>28%) to accommodate most changes in impedance, as the signal received at each position is influenced by the anatomical details of the gut and was different for every individual tested.

The natural movements of the tissues during respiration and other movements will influence the antenna input impedance, but this effect was not found to be significant. The inward-directed slot antenna is an excellent option for internal-to-surface body communications and may be used to improve the accuracy of the received signal level indicator (RSSI)-based method of pill localization.

In this series of experiments, the resonant frequency had a mean value of approximately 2.088 GHz. In a practical application, the slot antenna must be slightly modified (by slightly changing the structure of the brass feed and slot dimensions, bandwidth, and center frequency) so that the mean value of the resonant frequency lies at the ISM frequency 2.45 GHz for most positions on the body and for most body types. It is also evident that numerical modeling of the antenna impedance on the underlying tissue is not well matched to the in-vivo measurements. Despite this fact, we conclude that variations in the S_{11} are sufficiently low to allow for the accurate measurement of field strength.

The slot antenna is linearly polarized and thus is dependent on the orientation of the radio pill inside the human gut. For tracking applications, the orientation of the transmitting antenna will be different at different locations, so the radiation field pattern must be taken into account in the RSSI-based localization method [Salchak et al., 2020]. With these reservations, the slot antenna is sufficiently small and reliable for electric field strength measurements on the human body from a GI radio pill.

ACKNOWLEDGMENTS

The authors would like to thank the participants for volunteering to participate in the study. N. AlBadri thanks Griffith University for a postgraduate scholarship.

REFERENCES

Agarwal K, Guo YX, Salam B. 2016. Wearable AMC backed near-endfire antenna for on-body communications on latex substrate. IEEE Transactions on Components, Packaging and Manufacturing Technology 6:346–358.

Agneessens S, Lemey S, Vervust T, Rogier H. 2015. Wearable, small, and robust: The circular quarter-mode textile antenna. IEEE Antennas and Wireless Propagation Letters 14:1482–1485.

Albadri N, Espinosa HG, Thiel DV. 2020. Wearable slot antenna for biomedical applications: Mutual coupling and external interference. Radioengineering 29:285–290.

Arefin MS, Redouté JM, Yuce MR. 2018. Integration of low-power ASIC and MEMS sensors for monitoring gastrointestinal tract using a wireless capsule system. IEEE Journal of Biomedical and Health Informatics 22:87–97.

Arif A, Zubair M, Ali M, Khan MU, Mehmood M. 2019. A compact, low-profile fractal antenna for wearable on-body WBAN applications. IEEE Antennas and Wireless Propagation Letters 18:981–985.

Ashyap AYI, Abidin ZZ, Dahlan SH, Majid HA, Shaharil MS, Kamarudin M, Alomainy A. 2017. Compact and low-profile textile EBG-based antenna for wearable medical applications. IEEE Antennas and Wireless Propagation Letters 16:2550–2553.

Baghaee RM, Mohassel JR. 2016. Broadband explicit time domain model for human skin permittivity. IEEE Transactions on Microwave Theory and Techniques 64:2678–2683.

Caffrey CM, Chevalerias O, Mathuna CO, Twomey K. 2008. Swallowable-capsule technology. IEEE Pervasive Computing 7:23–29.

Deneris ZA, Pe'a DE, Furse CM. 2019. A layered pork model for subdermal antenna tests at 433 MHz. IEEE Journal of Electromagnetics RF and Microwaves in Medicine and Biology 3:171–176.

Fernández M, Espinosa HG, Thiel DV, Arrinda A. 2018a. Wearable slot antenna at 2.45 GHz for off-body radiation: Analysis of efficiency, frequency shift, and body absorption. Bioelectromagnetics 39:25–34.

Fernández M, Thiel DV, Arrinda A, Espinosa HG. 2018b. An inward directed antenna for gastro-intestinal radio pill tracking at 2.45 GHz. Microwave and Optical Technology Letters 60:1644–1649.

Fernández M, Espinosa HG, Guerra D, Peña I, Thiel DV, Arrinda A. 2020. RF energy absorption in human bodies due to wearable antennas in the 2.4 GHz frequency band. Bioelectromagnetics. 41:73–79.

Gabriel C. 1996. Compilation of the dielectric properties of body tissues at RF and microwave frequencies. Report N.AL/OE-TR-1996-0037, Occupational and Environmental Health Directorate, Radiofrequency Radiation Division, Brooks Air Force Base.

Hassan S. 2018. Overview of musculoskeletal ultrasound for the clinical rheumatologist. Clinical and Experimental Rheumatology 36:3–9.

Hides JA, Richardson CA, Jull GA. 1995. Magnetic resonance imaging and ultrasonography of the lumbar multifidus muscle: Comparison of two different modalities. Spine 20:54–58.

Kiourti A, Nikita KS. 2017. A review of in-body biotelemetry devices: Implantables, ingestibles, and injectables. IEEE Transactions on Biomedical Engineering 64:1422–1430.

Kissi C, Särestöniemi M, Kumpuniemi T, Sonkki M, Myllymäki S, Srifi MN, Raez CP. 2019. Directive low-band UWB antenna for in-body medical communications. IEEE Access 7:149026–149038.

Lin JC. 1974. A cavity-backed slot radiator for microwave biological effect research. Journal of Microwave Power 9:63–67.

Miah MS, Khan AN, Ichein C, Haneda K, Takizawa KI. 2019. Antenna system design for improved wireless capsule endoscope links at 433 MHz. IEEE Transactions on Antennas and Propagation 67:2687–2699.

Miklavcic D, Pavselj N, Hart FX. 2006. Electric properties of tissues. In: M. Akay Wiley Encyclopedia of Biomedical Engineering. Hoboken, NJ: John Wiley & Sons. pp 1–12.

Paracha KN, Rahim SKA, Soh PJ, Khalily M. 2019. Wearable antennas: A review of materials, structures, and innovative features for autonomous communication and sensing. IEEE Access 7:56694–56712.

Ruiz DRR, Garde JM, Legarda J. 2019. Planar textile off-body communication antennas: A survey. Electronics 8:714.

Sabban A. 2019. Compact wearable meta materials antennas for energy harvesting systems, medical and IOT systems. Electronics 8:1340.

Salchak YA, Espinosa HG, Thiel DV. 2020. Modelling the surface field from an ingested radio transmitter with an approximate attenuation model for gastroenterology investigations. IEEE Transactions on Biomedical Engineering 67:504–511.

Salgado AJ, Coutinho OP, Reis RL. 2004. Bone tissue engineering: State of the art and future trends. Macromolecular Bioscience 4:743–765.

Tajin MAS, Bashara O, Liu Y, Levitt A, Dion G, Dandekar KR. 2019. Efficiency measurement of the flexible on-body antenna at varying levels of stretch in a reverberation chamber. IET Microwave, Antenna and Propagation 14:154–158.

Zhu XQ, Guo YX, Wu W. 2016. A compact dual-band antenna for wireless body-area network applications. IEEE Antennas and Wireless Propagation Letters 15:98–101.